





Fig. 2. Alternating high voltage and signal planes of MEDUSA prior to assembly of the chamber.

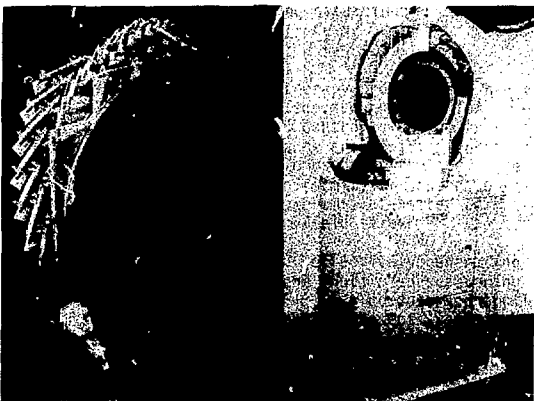
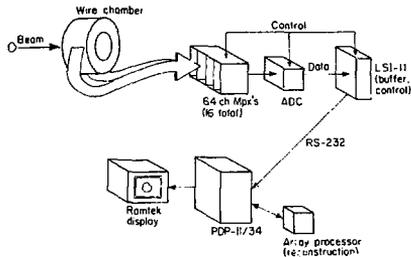


Fig. 3. a) Assembled chamber b) Chamber connected to electronics (data acquisition and LSI-11).

A block diagram of the electronics is shown in Figure 4. Ribbon cables connect the signal wires to the integrating capacitors on the 64 channel multiplex cards. After the end of the data collection period (established by the LSI-11) capacitor voltages are sequentially sampled, digitized and stored in buffer memory. Upon command, the buffer is serially transmitted to the host computer where the data are smoothed, normalized and finally reconstructed into the beam profile. Reconstruction into a 64 x 64 array (4 mm pixel size) is presently done on the PDP 11/34, and takes about 40 seconds. This time will soon be cut to just a few seconds when the array processor is brought on line. The algorithm employed for reconstruction is the Fourier convolution method<sup>7,9</sup> and is briefly described in the Appendix. Images are displayed on a Ramtek color CRT terminal attached to the 11/34, and can be viewed remotely by the accelerator operators to assist in beam tuning.

#### IMAGES

Figures 5 and 6 are examples of images produced by MEDUSA. Fig. 5a is an image of the beam before it has been broadened and shaped for therapy. Figure 5b is the fully shaped 20 cm diameter therapy beam before optimum tuning has been achieved, showing about an 8% intensity variation over the field. (The color display provides considerably more sensitivity than is visible in these figures.) Figures 6a and 6b were taken during initial commissioning studies of the chamber. A copper bar and lead brick were placed in front of the chamber so as to block out portions of the beam. The sharpness of the reconstructed edges is a good indication of the spatial resolution of the instrument (10% to 90% in 3 pixels), and of its ability to reconstruct



XBL 792-746

Fig. 4. Block diagram of information flow in MEDUSA.

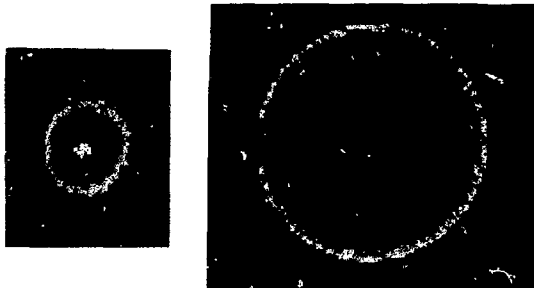


Fig. 5. Reconstructed images a) beam spot prior to shaping for therapy, b) shaped 20 cm therapy field before fine tuning to remove hot spot at upper corner.



Fig. 6. Field obstructed by metallic absorbers. Reconstructions performed a) prior to, and b) after smoothing of the raw data.

asymmetric patterns. The two figures are reconstructions of the same data set, before and after smoothing of the data. Data must be smoothed to compensate for mismatching in capacitor values and other components, as well as to average out statistical variations. The optimization of smoothing algorithms is still being researched.

#### CONCLUSIONS

MEDUSA has already proven to be a highly useful tool for heavy ion radiotherapy beam tuning and verification. In addition, it can be used for the measurement of a wide variety of beams, from x rays and electrons, to neutrons (with slight chamber modifications), and thus could find widespread applications in industrial and medical therapy beam monitoring.

## ACKNOWLEDGMENTS

We wish to thank R. Edwards and E. Stuart for mechanical design and fabrication of the chamber, D. Rondeau, R. Rozzano and the LBL Real Time Systems Group for the design and construction of the electronic portions of the system, and R.P. Singh and J. Llacer for programming help and general assistance in getting our software onto the Biomedical PDP 11/34 system.

## REFERENCES

1. J.R. Alonso, J. Howard, T. Criswell. Preceeding paper.
2. A.M. Koehler, R.J. Schneider, J.M. Sisterson, Med. Phys. 4 (1977), p. 297.
3. K. Crowe, L. Kanstein, J. Lyman, F. Yeater, LBL-4235, August 1975.
4. Ch. Leemann, J. Alonso, H. Grunder, E. Hoyer, G. Kalnins, D. Rondeau, J. Staples, F. Voelker, IEEE Trans. Nucl. Sci. NS-24 (1977), p. 1052
5. J. Cuperus, R. Morgado, IEEE Trans. Nucl. Sci. NS-22 (1975), p.1561.
6. J.S. Fraser, 5th Conf. on Applic. of Small Accel., Denton, Texas, November 1978.
7. See for example, I A. Shepp, B.F. Logan, IEEE Trans. Nucl. Sci. NS-21 (1974), p. 21.
8. R.H. Huesman, Phys. Med. and Biol 22 (1977), p. 511.
9. L. Wang, The Aerospace Corp. Report ATR-75 (8139)-1 (1975).
10. Z.H. Cho, IEEE Trans. Nucl. Sci. NS-21 (1974), P. 44.

## APPENDIX

### Fourier Convolution Reconstruction Algorithm

If we express the two-dimensional beam intensity profile as  $I(x,y)$  in Cartesian coordinates, the electric charges collected on any given wire of the wire chamber is a line integral of  $I(x,y)$  over that particular wire. (Actually it is proportional to the integrated value of  $I(x,y)$  covered by the length of the wire and the width extending midway toward the adjacent wires.) If the normal to the wire through the origin makes an angle  $\theta$  with the positive  $x$ -axis and the wire is at a distance  $t$  away from the origin, as shown in Figure 1, the equation of the wire is:

$$L(t,\theta) : x \cos\theta + y \sin\theta = t \quad (1)$$

The line integral of  $I(x,y)$  over the wire is then,

$$\begin{aligned} P(t,\theta) &= \int_{L(t,\theta)} I(x,y) \, ds \\ &= \int_{-\infty}^{\infty} \int_{-\infty}^{\infty} I(x,y) \delta(x \cos\theta + y \sin\theta - t) \, dx \, dy \end{aligned} \quad (2)$$

where  $\delta(x)$  is the Dirac delta function. We define the two-dimensional Fourier transform of the beam profile,  $I(x,y)$ , as

$$\begin{aligned} \hat{I}(\omega,\theta) &= \\ \int_{-\infty}^{\infty} \int_{-\infty}^{\infty} I(x,y) e^{-i\omega(x \cos\theta + y \sin\theta)} \, dx \, dy \end{aligned} \quad (3)$$

and the Fourier transform of  $P(t,\theta)$  as

$$\hat{P}(\omega,\theta) = \int_{-\infty}^{\infty} e^{-i\omega t} P(t,\theta) \, dt \quad (4)$$

The relationship between the two Fourier transforms which forms the basis of the reconstruction algorithm, is shown below.

$$\hat{P}(\omega,\theta) = \hat{I}(\omega,\theta). \quad (5)$$

If  $P(t,\theta)$  is known for all  $t$  and  $\theta$ , then the inverse Fourier transform gives  $I(x,y)$  as

$$\begin{aligned} I(x,y) &= \frac{1}{4\pi^2} \int_0^\pi \int_{-\infty}^{\infty} \hat{P}(\omega,\theta) \cdot \\ &e^{i\omega(x \cos\theta + y \sin\theta)} |\omega| \, d\omega \end{aligned} \quad (6)$$

$$\begin{aligned} &= \frac{1}{4\pi^2} \int_0^\pi \int_{-\infty}^{\infty} \int_{-\infty}^{\infty} P(t,\theta) \cdot \\ &e^{i\omega(x \cos\theta + y \sin\theta - t)} |\omega| \, d\omega \end{aligned} \quad (7)$$

The integrand diverges when the range of  $\omega$  extends from  $-\infty$  to  $\infty$ ; however, if the Fourier transform  $\hat{P}(\omega,\theta)$  is band-limited,  $I(x,y)$  can be approximately evaluated.

In our wire chamber, the line integrals  $P(t,\theta)$  over the wires are known only over the discretely placed wires (64 wires per plane) at finite angular orientations (16 planes cover  $\pi$  radians at  $\pi/16$  radian intervals). The line integrals are then written as  $P(t_m, \theta_n)$ , with  $t_m = (m-32.5)d$ ,  $m = 1, 2, \dots, 64$ , and  $d$  is the wire spacing (4 mm); and  $\theta_n = n\pi/N$ ,  $n = 0, 1, \dots, 15$ , and  $N = 16$ . Then the beam intensity profile is approximately evaluated by replacing the integrals in (7) by sums.

$$\begin{aligned} I_\phi(x,y) &= \frac{d}{2N} \sum_{n=0}^{N-1} \sum_{m=1}^{64} P(t_m, \theta_n) \cdot \\ &\phi(x \cos\theta_n + y \sin\theta_n - t_m) \end{aligned} \quad (8)$$

The subscript  $\phi$  of  $I_\phi$  in the above expression indicates the dependence of  $I_\phi(x,y)$  over the weighting function of  $\phi$  used in the computation. The meaning of  $\phi$  is described below. The intensity  $I(x,y)$  at  $(x,y)$  which lies on the line  $L(t_\ell, \theta_n)$ , when reconstructed by back-projecting  $P(t_\ell, \theta_n)$ , is blurred unless properly compensated by all other  $P(t_m, \theta_n)$  values. The function  $\phi$  establishes this mixing, and thus gives the extent to which each of the  $m$  wires contributes to the  $\ell$ th wire. This functional relationship can take various forms depending on the reconstruction algorithm employed; for the Fourier convolution method used here the compensated points  $P'(t_\ell, \theta_n)$  are given as follows,<sup>9</sup> where now  $t_m$  is expressed as  $(m - 32.5)d$ .

$$\begin{aligned} P'(\ell d, \theta_n) &= \frac{1}{4d} P(\ell d, \theta_n) - \\ &\frac{1}{\pi^2 d} \sum_{m=\text{odd}} P\{(\ell+m)d, \theta_n\} / m^2 \end{aligned} \quad (9)$$

The beam intensity profile is then given by back-projection of these values;

$$\begin{aligned} I(x,y) &= \frac{d}{2N} \sum_{n=0}^{N-1} \sum_{\ell=1}^{64} P'(\ell d, \theta_n) \cdot \\ &\delta(x \cos\theta_n + y \sin\theta_n - \ell d). \end{aligned} \quad (10)$$

In actual computation,  $I(x,y)$  is evaluated over the  $64 \times 64$  matrix of square areas of  $d^2$ , i.e.,  $I(x_i, y_j)$  at  $x_i = id$ ,  $i = 1, 2, \dots, 64$ , and  $y_j = jd$ , and  $j = 1, 2, \dots, 64$ , with  $d = 4$  mm. Since an arbitrary matrix element  $(x_i, y_j)$  may include contributions from up to three  $P'(\ell d, \theta_n)$ , additional geometric compensating factors<sup>10</sup> must be used in the back-projection computation.